IL NUOVO CIMENTO **44 C** (2021) 5
DOI 10.1393/ncc/i2021-21005-x

COMMUNICATIONS: SIF Congress 2020

SiC detectors for nuclear fragment identification in heavy-ion collisions

C. CIAMPI([1])([2]) for the SICILIA COLLABORATION

([1]) *INFN, Sezione di Firenze - Firenze, Italy*
([2]) *Dipartimento di Fisica e Astronomia, Università di Firenze - Firenze, Italy*

received 24 January 2021

Summary. — Three different configurations of ΔE-E telescopes featuring SiC (Silicon Carbide) detectors have been employed for the identification of nuclear fragments produced in the ^{40,48}Ca+^{12}C interaction at 40 A MeV. Both the ΔE-E and PSA (Pulse Shape Analysis) techniques have been applied, and their results are here presented. The performance of the SiC detector prototypes in terms of identification capability is found to be comparable to that of state-of-the-art silicon detectors.

1. – Introduction

A new frontier for nuclear physics experiments is the study of very rare nuclear phenomena: due to the low cross sections involved, these experiments, *e.g.*, NUMEN [1], require a high beam intensity in order to collect a reasonable statistics of events within the available beam time. Semiconductor detectors are often the best choice for these applications, thanks to many favourable characteristics, such as their high resolution and excellent fragment identification capabilities. However, state-of-the-art silicon detectors may not be able to operate under such harsh environment due to the serious limitations they have in terms of radiation hardness [2].

Silicon carbide (SiC) is a wide band gap semiconductor, which represents an attractive alternative to silicon. In fact, it is characterised by the same excellent properties of silicon detectors (resolution, efficiency, linearity, compactness), combined with a larger radiation hardness [3]. It also features better temperature stability and insensitivity to visible light, and these characteristics can be extremely useful for their application in experiments performed in a hot plasma environment, such as NuReLP [4]. Nevertheless, SiC detectors having the characteristics required by the already cited NUMEN, NuReLP and other nuclear physics experiments, such as FAZIA [5] and ELIMED [6], are not yet commercially available. In this framework, the SiCILIA Collaboration has started [7]: the aim of the project was the development of new silicon carbide production technologies, in order to manufacture a set of thick SiC detectors with large area and high purity [8,9].

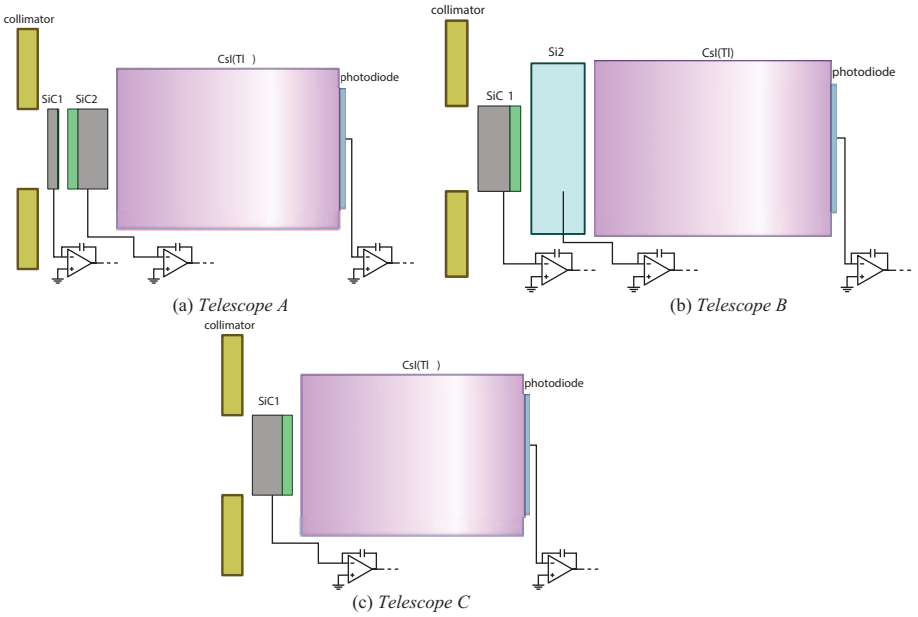

Fig. 1. – Sketches of the three telescope configurations. The light-green areas represent the SiC active layers, while the grey ones are their substrates. The collimator is shown in ochre, the Si detector in light blue and the CsI(Tl) scintillator in purple.

Different SiC detector prototypes have been produced within the SiCILIA project up to now: their active layer is either 10 μm or 100 μm thick, epitaxially grown on a 100 μm or 300 μm thick SiC substrate, respectively. Both p/n junction and Schottky configurations have been produced, on an active area of $0.5 \times 0.5\,\mathrm{cm}^2$ or $1.0 \times 1.0\,\mathrm{cm}^2$.

In the present work, some of the newly produced p/n junction SiC detector prototypes were mounted in a ΔE-E telescope configuration in order to study their suitability for ion identification exploiting both ΔE-E [10] and Pulse Shape Analysis [11-14] methods. To our knowledge, this is the first time that silicon carbide detectors are used for nuclear fragment identification. The experimental setup and the three different telescope configurations are described in sect. 2. In sect. 3 the data analysis procedure will be explained and the results of the application of both ΔE-E and PSA techniques will be presented. In sect. 4 conclusions will be drawn.

2. – Experimental setup

The three different telescope configurations inspected in this test are sketched in fig. 1 and are here described.

- Telescope A consists of three stages: the first one is a 10 μm thick SiC detector (A-SiC1), the second one is a 100 μm thick SiC detector (A-SiC2), and the third is a 10 cm thick CsI(Tl) scintillator read out by a photodiode (A-CsI). The first detector is reverse mounted (*i.e.*, low-field side facing the target), while the second one is front mounted, in order to avoid dead layers between the ΔE and the E stage of the telescope. This choice leaves a 300 μm thick dead layer between the active layer of the second and the third stage. The electrode on the active area of

TABLE I. – *Characteristics of the SiC prototypes employed in the test.*

	A-SiC1	A-SiC2	B-SiC1	B-SiC1bis	C-SiC1a,b
Thickness (μm)	10	100	100	100	100
Pads	1	4	3	1	2
Dep. Voltage (V)	4	400–700	25	25	400–700
Appl. Voltage (V)	50	150	150	40	150
Leakage Current (nA)	< 1	< 1	< 1	16	< 1

the 100 μm thick SiC detector A-SiC2 is divided into four equal pads, that have been connected to a single read-out chain.

- Telescope B is made of three stages as well: the ΔE stage is a reverse-mounted 100 μm thick SiC detector (B-SiC1), the second stage is a 500 μm thick silicon detector (B-Si2), and the third stage is a 10 cm thick CsI(Tl) scintillator. Also in this case, the electrode of B-SiC1 is divided into four pads: three of them are connected together, while the remaining one is connected to its own read-out chain (B-SiC1bis) due to the fact that this defective pad undergoes breakdown at only 40 V of applied bias.

- Telescope C features only two detection stages: the ΔE stage is a 100 μm thick SiC prototype (C-SiC1), reverse mounted, and the E stage is a CsI(Tl) scintillator (C-CsI). In this case, the four pads of C-SiC1 have been connected two by two, to two read-out chains: the two sections of the detector will be referred to as C-SiC1a and C-SiC1b.

The main parameters of the SiC detectors employed in this test are reported in table I. Only SiC detector prototypes with active area $1.0 \times 1.0\,\mathrm{cm}^2$ have been employed in this work. The Si detector and all the CsI(Tl) scintillators are the same kind of detectors that are used in the FAZIA apparatus [5], and their active areas are $2.0 \times 2.0\,\mathrm{cm}^2$ and $2.05 \times 2.05\,\mathrm{cm}^2$, respectively. Since the active area of the SiC prototypes is smaller, a 3 mm thick brass collimator has been placed in front of each telescope in order to select a $0.9 \times 0.9\,\mathrm{cm}^2$ area at the centre.

The telescopes were mounted inside the CICLOPE scattering chamber at the Laboratori Nazionali del Sud (LNS, Catania), together with the FAZIA apparatus. They were positioned at a polar angle of about 8°, at a distance of about 80 cm from the target. The reactions employed for the test were ^{40,48}Ca+^{12}C at 40 A MeV.

Each one of the detectors assembled in the telescopes was connected to its own read-out chain, based on a charge preamplifier of the same kind as those employed in the GARFIELD+RCo apparatus [15]. The output of the charge preamplifier has been digitized by means of custom digitizing boards originally designed for GARFIELD+RCo: each channel features a 125MSPS 14-bit sampling ADC, with a variable gain input stage and anti-aliasing filter. The acquired signals have been stored on a PC for the offline analysis.

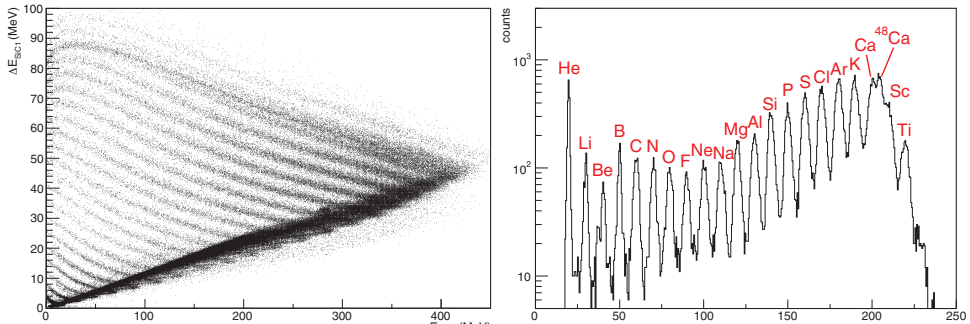

(a) Δ *E-E correlation* (b) *PI spectrum*

Fig. 2. – Panel (a): ΔE-E identification obtained with telescope A (A-SiC1 *vs.* A-SiC2). Veto imposed on A-CsI. Panel (b): PI spectrum for ΔE-E in panel (a).

3. – Analysis and results

The digitized signals have been analysed with Digital Signal Processing techniques. A unit gain trapezoidal filter has been applied to the baseline-subtracted signals for the amplitude extraction (*i.e.*, energy information). The rise time of the signals has been obtained by applying digital Constant Fraction Discriminators (dCFDs) based on cubic interpolation. The current signals for PSA, that were not originally acquired, have been obtained via a digital differentiation of the smoothing-spline interpolated charge signals [16].

3˙1. ΔE-E *technique.* – The ΔE-E correlation obtained with telescope A (A-SiC1 *vs.* A-SiC2) is shown in fig. 2. The different correlation ridges corresponding to the various elements are clearly visible: the telescope is able to resolve elements up to $Z = 22$, which are the heaviest products for the employed reaction. A veto condition on the amplitude of the A-CsI signal has been imposed in order to exclude punch-through events, *i.e.*, particles not stopped in the second stage: it is clear that the veto condition is not able to eliminate all the punch-through events from the plot. This is due to the particles punching through the active layer of A-SiC2 and stopping in the 300 μm dead layer behind, that do not produce any signal in the scintillator. The details of the calibration can be found in ref. [17].

In order to express quantitatively the Z resolution of the telescope, we applied the linearization procedure of the ΔE-E correlation, as illustrated in ref. [18]: a Particle Identification (PI) value is assigned to each event, based on the position of its ΔE-E point with respect to the two adjacent Z-lines, previously drawn on the correlation ridges. The PI values distribution obtained with telescope A is reported in fig. 2. Here, the punch-through events have been excluded through a graphical cut. The peaks corresponding to different elements are readily visible: the separation between them is usually quantified by means of a Figure of Merit (FoM) [19]. Conventionally, a FoM greater than 0.7 between two peaks indicates that they are sufficiently well separated. A table containing all the FoM values obtained with telescope A can be found in ref. [17]: the FoM is greater than 0.7 for all the elements, except for the separation between Ca and Sc, due to the high intensity of the ^{48}Ca peak (the projectile of the reaction). This result confirms that telescope A has good Z identification capability, but it does not resolve

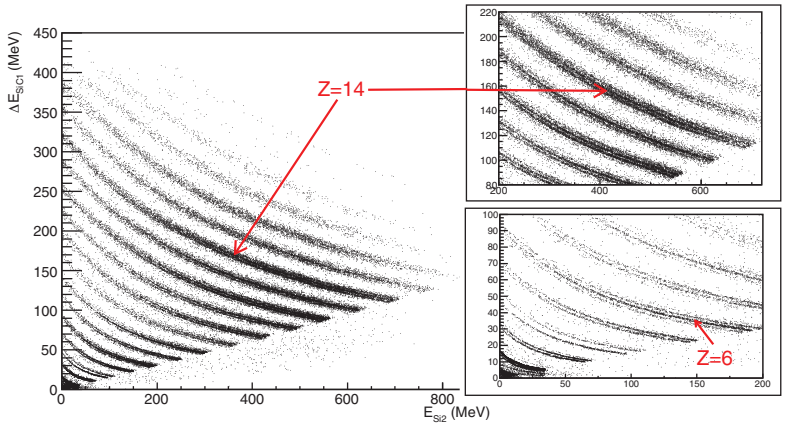

Fig. 3. – ΔE-E correlation obtained with telescope B (B-SiC1 *vs.* B-Si2). Veto imposed on B-CsI. The two insets on the right side show two enlarged sections of the graph, around $Z = 14$ (top) and $Z = 6$ (bottom).

the single isotopes. The lack of isotopic identification can be a consequence of the energy straggling in the 10 μm thick first stage (an effect that has already been observed for thin ΔE detectors [20]), and/or of electronic noise. In order to understand the role of these two contributions, we simulated ΔE-E correlations including only these two worsening effects on the resolution. We found a discrepancy between the experimental FoM values and the simulated ones, indicating that the experimental performance is affected by some other effects. The intrinsic limit due to the energy straggling has not been reeached, and there is room for further improvement. However, it is worth noting that a ΔE stage detector as thin as A-SiC1 allowed to reach an energy threshold for Z identification as low as 1.5 A MeV.

A very good Z identification capability is obtained with telescope B, as is evident from the ΔE-E correlation (B-SiC1 *vs.* B-Si2) shown in fig. 3. On closer inspection, one can also notice isotopic separation within the various Z ridges, up to $Z \sim 14$. Due to the thicker ΔE stage, we obtained a better identification performance, but also a higher identification threshold. Also in this case, we exploit a veto condition on the signal of the third stage detector (B-CsI) to exclude punch-through events. Unlike telescope A, telescope B has no dead layer between the second and the third stage, hence the effectiveness of the punch-through suppression. By applying the aforementioned linearization procedure, we obtain the PI value distributions in fig. 4: we reported four different Z intervals in which isotopic identification is achieved, as can be seen from the multiple peak structure of each element. We obtained a FoM ≥ 0.7 for all the detected isotopes up to $Z \sim 14$ (the complete list of the FoM values between different isotopes can be found in ref. [17], table 4, together with some information on the calibration procedure).

Telescope C is the only two-stage telescope that has been tested in this work. In fig. 5, the ΔE-E correlation between C-SiC1b and C-CsI is shown, and the corresponding PI histogram obtained through the linearization procedure is reported in fig. 5. A good element identification is achieved, and also some isotopic identification for $Z \lesssim 3$, in a limited energy range. We obtained a FoM greater than 0.7 for all the detected elements.

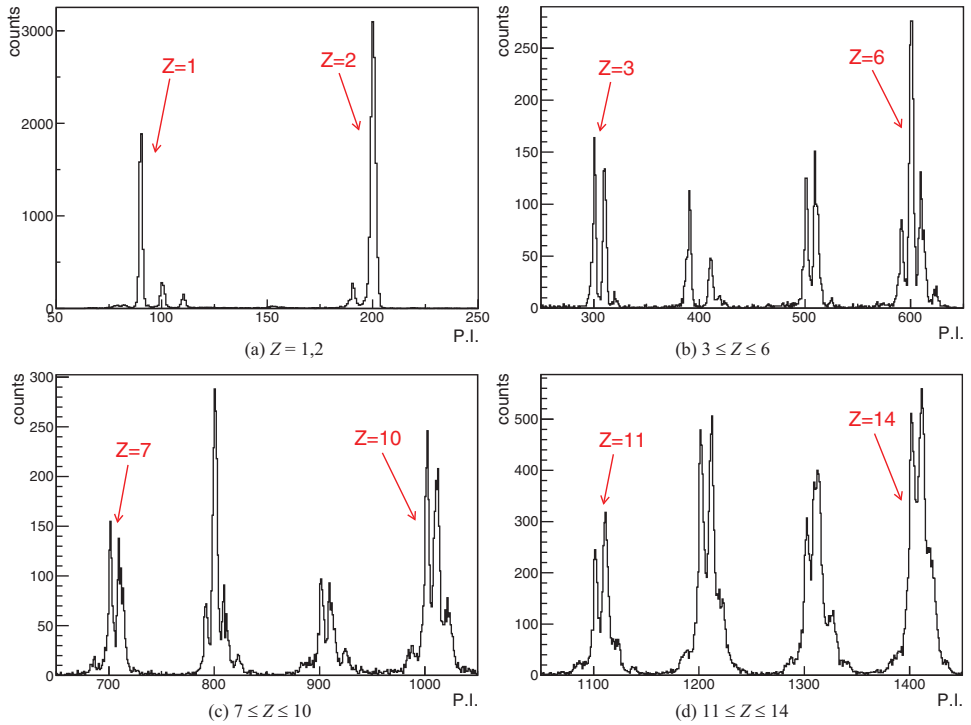

(a) $Z = 1,2$ (b) $3 \leq Z \leq 6$

(c) $7 \leq Z \leq 10$ (d) $11 \leq Z \leq 14$

Fig. 4. – Details of the PI spectrum obtained from the correlation in fig. 3. Each different peak corresponds to a different isotope.

Since after the experiment it was found that C-SiC1a,b did not operate in a full depletion condition during the measurements, it can be asserted that there may be room for improvement.

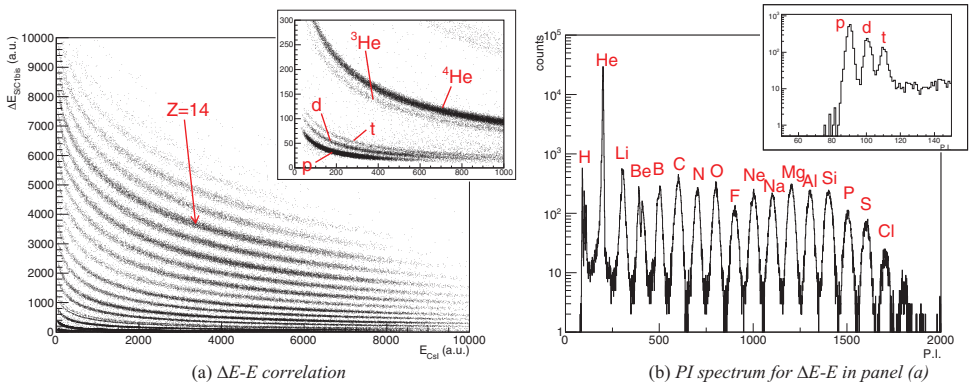

(a) *ΔE-E correlation* (b) *PI spectrum for ΔE-E in panel (a)*

Fig. 5. – ΔE-E identification obtained with telescope C (C-SiC1b *vs.* C-CsI). This telescope has not been calibrated due to the fact that after the experiment it was found that C-SiC1a,b did not operate in a full depletion condition during the measurements.

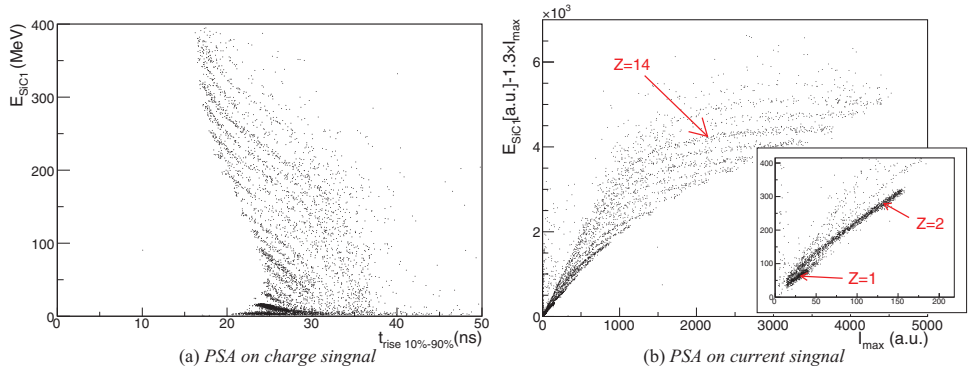

(a) *PSA on charge singnal* (b) *PSA on current singnal*

Fig. 6. – Pulse shape identification applied to the fragments stopped in B-SiC1. The plots are obtained by imposing a veto condition on the second stage of the telescope B-Si2.

3˙2. *Pulse shape analysis*. – The pulse shape identification capability was tested on the first stage of telescope B, namely B-SiC1 and B-SiC1bis. We recall that this detector is reverse mounted: this is the most suitable configuration for this kind of applications, as demonstrated in ref. [21].

Two correlation graphs, built exploiting two different PS related observables, are here presented. In fig. 6(a) the correlation graph of the energy *vs.* the 10%–90% rise time of the charge signal (charge preamplifier output) obtained with B-SiC1 is reported. Figure 6(b) shows the correlation between the value $E - 1.3I_{max}$ and the maximum of the current signal I_{max} (extracted from the charge signal via digital signal processing) obtained with B-SiC1. The choice of the value reported on the ordinate axis, instead of just the energy value, was made to "open up" the correlation graph. In both plots, the correlation ridges corresponding to different elements are readily recognizable. We therefore proceeded with the linearization procedure previously described, thus obtaining the PI value histograms reported in fig. 7. The FoM is found to be greater than 0.7 for all the considered element pairs.

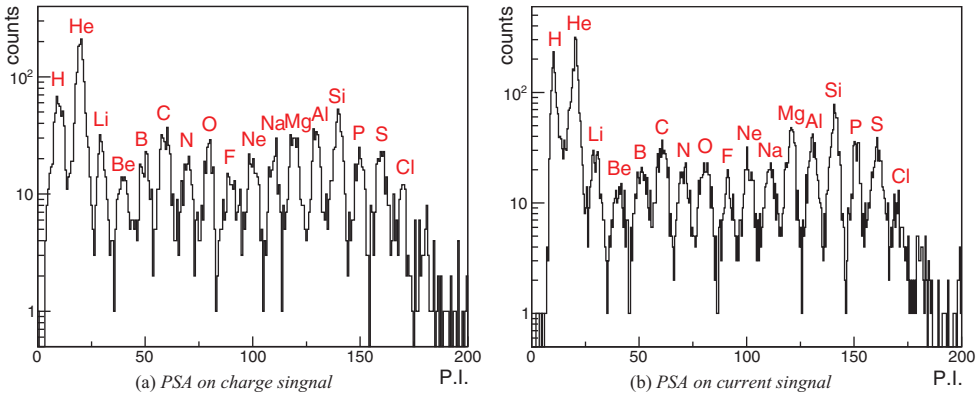

(a) *PSA on charge singnal* (b) *PSA on current singnal*

Fig. 7. – PI spectra obtained with pulse shape identification applied to the fragments stopped in B-SiC1.

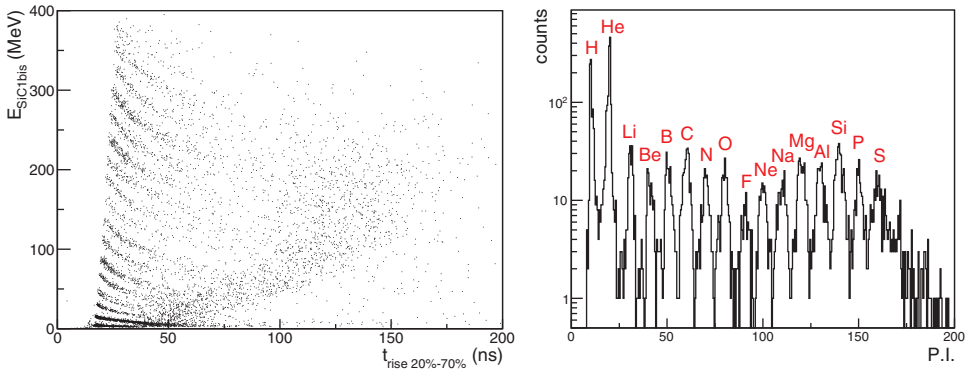

(a) *Energy vs. Rise time (20-70%)* (b) *PI spectrum obtained from panel (a)*

Fig. 8. – Pulse shape identification for the fragments stopped in B-SiC1bis. A veto condition on the second stage of the telescope B-Si2 was imposed.

In ref. [22] it has been observed that a better PSA performance is achieved with silicon detectors by lowering the applied voltage close to the depletion voltage. If the same consideration stands also for SiC detectors, the performance of B-SiC1 should be far from optimal: in fact, as can be seen from the values reported in table I, detector B-SiC1 was six times overbiased. However, the pad of the same first stage detector, referred to as B-SiC1bis, was biased with a lower voltage, and it therefore operated overbiased by a lower factor. In fig. 8(a) the correlation graph between energy and rise time 20%–70% obtained for the particles stopped in B-SiC1bis is shown. The PI spectrum obtained from the linearization procedure is presented in fig. 8(b). The two panels of fig. 9 show the expanded views of the same two plots over the region of light charged particles, where even some isotopic resolution is achieved. The FoM values obtained with PSA on B-SiC1bis are greater than 0.7 for all the element pairs, and higher than those obtained with both PSA methods on B-SiC1. The complete lists of the FoM values obtained with PSA techniques applied to particles stopped in detector B-SiC1 and B-SiC1bis is

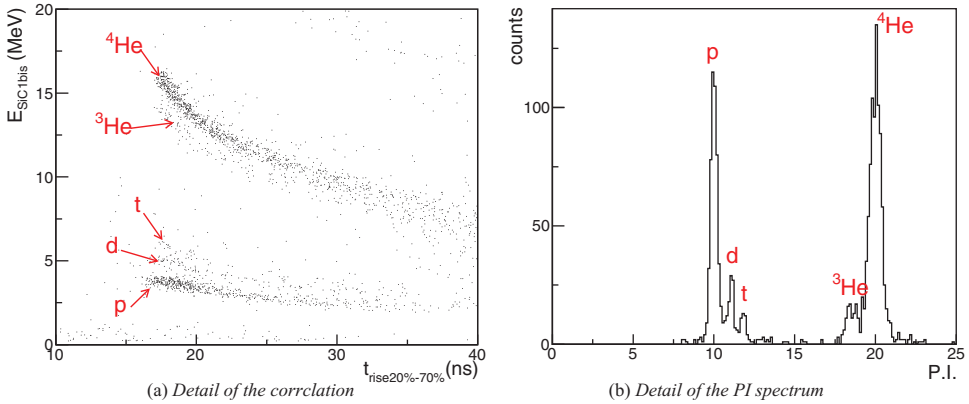

(a) *Detail of the corrclation* (b) *Detail of the PI spectrum*

Fig. 9. – Pulse shape identification for the fragments stopped in B-SiC1bis. Details of the region of light charged particles are given in panel (a) in terms of correlation spectrum, in panel (b) in terms of PI spectrum.

available in ref. [17]. These findings confirm the better performance that we expected for the lower biased SiC detector. However, a systematic study of the PSA performance as a function of the applied bias has been planned.

4. – Conclusions

The behaviour of some 4H-SiC detector prototypes produced within the SiCILIA project has been studied. We focused on the performance of the newly produced detectors in terms of ion identification capability: for the first time, in this work, SiC detectors have been employed in a ΔE-E telescope configuration, in view of their use in the next-generation nuclear physics experiments. Three different telescope arrangements have been tested exploiting a ^{40,48}Ca beam at 40 A MeV on a ^{12}C target.

The first telescope, referred to as telescope A, had a (10 μm SiC)–(100 μm SiC)-CsI configuration. With this setup, we obtained good element identification up to $Z \sim 22$, but no isotopic separation. Thanks to the thin first-stage detector the energy threshold for identification was as low as $\sim 1.5\,A$ MeV. By performing some simulations, we verified that the intrinsic physical limit imposed by the energy straggling in such a thin first stage has not been reached, and there is still room for improvement.

The configuration of telescope B was (100 μm SiC)–(500 μm Si)-CsI. With this arrangement we achieved a well-defined element identification up to $Z \sim 20$ (the heavier fragment collected with enough statistics, due to the reaction kinematics). For all the elements up to $Z = 14$ also a good isotopic identification has been achieved.

The third telescope was the only two-stage configuration, namely (100 μm SiC)-CsI. Also in this case we obtained a good element separation for all the fragments up to $Z \sim 20$. Isotopic identification has been achieved for elements up to berillium in a limited energy interval.

We also evaluated the performance of the SiC detector prototypes in terms of ion identification via PSA, a useful technique for identifying nuclear fragments stopped within a semiconductor detector. The results of the PSA identification technique on the 100 μm thick SiC detector B-SiC1 are promising. In fact, we obtained a good element identification, though without mass separation. However, some isotopic identification for hydrogen and helium isotopes was obtained with the SiC detector pad referred to as B-SiC1bis. This pad was biased at a lower voltage than B-SiC1, thus possibly causing its better performance. Further studies are planned in this regard, including a careful evaluation of the energy threshold for identification.

Further measurements have already been made, and the data analysis is still ongoing. The radiation hardness of the SiC detector prototypes produced within the project is being studied. A study of their charge collection efficiency, including a comparison with model predictions, is also planned. A study of their behaviour under neutron irradiation has been published in ref. [23]. A 10 μm thick SiC prototype has also been characterised for dosimetric applications [24].

REFERENCES

[1] Cappuzzello P. *et al.*, *Eur. Phys. J. A*, **54** (2018) 72.
[2] Barlini S. *et al.*, *Nucl. Instrum. Methods Phys. Res. A*, **707** (2013) 89.
[3] Raciti G. *et al.*, *Nucl. Phys. A*, **834** (2010) 784c.
[4] Negoita F. *et al.*, *Rom. Rep. Phys.*, **68** (2016) S37.
[5] Bougault R. *et al.*, *Eur. Phys. J. A*, **50** (2014) 47.

[6] Cirrone G. A. P. *et al.*, *Nucl. Instrum. Methods Phys. Res. A*, **730** (2013) 174.
[7] Tudisco S. *et al.*, *Sensors*, **18** (2018) 2289.
[8] Tudisco S. *et al.*, *Nuovo Cimento C*, **42** (2019) 74.
[9] La Via F. *et al.*, *J. Phys.: Conf. Ser.*, **1561** (2020) 012013.
[10] Knoll G.F., *Radiation Detection and Measurement* (Wiley) 2010.
[11] England J. *et al.*, *Nucl. Instrum. Methods Phys. Res. A*, **280** (1989) 291.
[12] Pausch G. *et al.*, *Nucl. Instrum. Methods Phys. Res. A*, **322** (1992) 43.
[13] Ammerlaan C.A. *et al.*, *Nucl. Instrum. Methods*, **22** (1963) 189.
[14] Mutterer M. *et al.*, *IEEE Trans. Nucl. Sci.*, **47** (2000) 756.
[15] Bruno M. *et al.*, *Eur. Phys. J. A*, **49** (2013) 1.
[16] Ottanelli P., PhD Thesis, Università di Firenze (2019).
[17] Ciampi C. *et al.*, *Nucl. Instrum. Methods Phys. Res. A*, **925** (2019) 60.
[18] Bardelli L. *et al.*, *Nucl. Instrum. Methods Phys. Res. A*, **654** (2011) 272.
[19] Winyard L.A. *et al.*, *Nucl. Instrum. Methods Phys. Res.*, **95** (1971) 141.
[20] Kordyasz A.J., *Eur. Phys. J. A*, **51** (2015) 15.
[21] Le Neindre N. *et al.*, *Nucl. Instrum. Methods Phys. Res. A*, **701** (2013) 145.
[22] Pasquali G. *et al.*, *Eur. Phys. J. A*, **50** (2014) 86.
[23] Rebai M. *et al.*, *Nucl. Instrum. Methods Phys. Res. A*, **926** (2019) 162637.
[24] Petringa G. *et al.*, *J. Instrum.*, **15** (2020) C05023.